JOURNAL OF COMPUTATIONAL PHYSICS 97, 444–459 (1991)

A New Semi-implicit Method for MHD Computations

K. LERBINGER AND J. F. LUCIANI

Centre de Physique Théorique de l'Ecole Polytechnique,
91128 Palaiseau Cedex, France

Received January 31, 1990; revised May 16, 1990

An efficient semi-implicit method for the solution of the nonlinear, three-dimensional, resistive MHD equations is presented. The method is unconditionally stable with respect to the compressional fast magnetoacoustic and shear Alfven waves. The time step is limited instead by the nonlinear physical plasma phenomena. Furthermore, the method allows a high spatial resolution. Physically relevant test cases are presented and the feasibility of longtime simulations is discussed. © 1991 Academic Press, Inc.

I. INTRODUCTION

The equations of nonideal magnetohydrodynamics (MHD) are widely used to study the macroscopic behaviour of toroidal or linear plasma confinement devices. One area of application is the study of plasma evolution leading to major disruptions, another area is the sawtooth oscillations in the ohmic regime of tokamaks. As this is one of the types of behaviour we want to simulate with the method we have developed we shall give a brief description of this interesting plasma phenomena.

The "ramp-up phase" of the sawtooth is a slow diffusion of the whole plasma configuration on the resistive time scale, its duration is about 10–100 ms, until a threshold is reached, whose exact characterisation is yet unknown. After reaching the threshold there is a sudden crash on a time scale of about 100 μs, characterised by an expulsion of central thermal plasma energy toward the border of the discharge, a sudden fall of the central electron temperature, and magnetic reconnection around a specific surface. This whole process is repeated periodically.

The whole sawtooth cycle is not only characterized by disparate time scales, where the slowest scale is long compared to those associated with the fastest normal modes of the system, but also by very narrow current spikes governing the dynamics of the magnetic reconnection. Therefore a numerical scheme should obviously be stable for large time steps, as these are necessary for the "ramp-up phase" and, on the other hand, guarantee a high spatial resolution for correctly describing the magnetic reconnection process without a prohibitive number of radial grid points.

The first MHD simulations of tokamak discharges made use of the reduced

0021-9991/91 $3.00

MHD equations [1]; early calculations have retained only the leading order terms in the aspect ratio expansion [2, 3], while later, higher order corrections have been included [4]. Another approach assumed the fluid flow to be incompressible [5]. In both models, the compressional fast magnetoacoustic waves with highest frequencies about τ_a/ε are removed from the system (τ_a being the Alfven time corresponding to the transit of an Alfven wave around the torus in the strong toroidal magnetic field, ε being the grid spacing). It should be remarked that for the model with incompressible plasma flow one needs a self-consistent definition of pressure, which could lead to nonphysical behaviour during the crashes, and for resistive instabilities, it can change the stability threshold. The time advance is made by an explicit scheme, limiting the time step by a shear Alfven Courant–Friedrichs–Lewy (CFL) constraint: $\Delta t < \tau_a/M$, where M is the highest poloidal Fourier mode. This is quite an improvement over the time step restriction caused by the fast waves which exist in the complete system but this shear Alfven constraint is still prohibitive for long time (10^3–$10^4\tau_a$) simulations in three dimensions. The solution to eliminate all CFL constraints by use of an implicit time advance, while in principle possible in three dimensions, would require the solution, every time step, of matrix systems to large to be feasible.

In Ref. [6, FAR code], the full compressible toroidal equations are solved in the following way: linearly, the scheme is fully implicit; this requires an inversion of 2D matrices systems that is feasible in the MHD case by present computers. Nonlinearly, an explicit diffusion term is added that damps the compressible part of the velocity. In this way, nonlinear computations with rather high time steps are possible (see part II.E for a comparison between this scheme and ours).

Recently, different methods have been developed in order to solve the full compressible MHD equations in three dimensions without CFL time step restrictions [7–10]. The most promising one seems to be the semi-implicit method, introduced and further refined by Harned and collaborators [8–10]. The basic idea of these semi-implicit schemes is to add new terms to the MHD equations to slow down artificially only the highest compressional modes or both the compressional and shear Alfven modes. These additional terms vanish as $\Delta t \to 0$, but they give a numerical algorithm which in the first case is unconditionally stable with respect to the fast modes, limited only by a shear Alfven CFL constraint and unconditionally stable in the second case. The slowing down of the modes is obtained by replacing the equation of motion $v = F$ by a "semi-implicit" equation $(1 - \Delta t^2 L)v = F$, where L is an elliptic operator which dominates the explicit part. L can be taken to be the Laplacian, or another anisotropic elliptic operator.

This method has proved its efficiency, but has an obvious limitation: as L must dominate the explicit normal modes in the whole magnetic field, accuracy is generally obtained with a time step $\Delta t \ll \tau_a$. With time steps of the order $\Delta t = \tau_a$ or larger, current spikes as those arising around resonant surfaces are broadened unacceptably, and accuracy on linear modes is lost.

The numerical scheme we have developed is based on the same idea, i.e., to slow down artificially the high frequency waves. This is obtained by using the fact that

the equilibrium magnetic fields dominate the magnetic perturbations; this also is the reason why longtime-simulations have to be run to study the macroscopic behaviour of tokamak plasmas. Therefore, we propose a semi-implicit method which is

— linearly fully implicit, the implicit matrices being one-dimensional in cylindrical geometry and two-dimensional in toroidal geometry

— in the nonlinear phases, the numerical system is stabilized by an elliptic operator, added to the fully implicit linear operator. This elliptic operator dominates only the nonlinear magnetic perturbations, and thus its size is much smaller (10^{-3}–10^{-4}) than that of the elliptic operator used in the above semi-implicit methods. In this way we have found that the time step can adjust itself to the actual nonlinear situation as the relevant physical time scale.

As is evident this scheme is more difficult to implement than the currently proposed semi-implicit methods, especially in toroidal geometry. Furthermore, the computation time per time step is larger in toroidal geometry. However, the gain in spatial resolution is considerable, allowing simulations which would otherwise be impossible with the same spatial precision.

We shall present the numerical scheme in Section II, together with a comparison with previous work; results of numerical tests in cylindrical geometry are presented and discussed in Section III. Conclusions are stated in Section IV, where pros and cons of the method are discussed.

II. The Numerical Scheme

II.A. *The MHD Equations*

The resistive, compressible MHD equations written in non-dimensional form are

$$\rho(\dot{\mathbf{v}} + (\mathbf{v}\cdot\nabla)\mathbf{v}) = \mathbf{j}\times\mathbf{b} - \nabla p + \nu\,\Delta\mathbf{v} \tag{1}$$

$$\dot{\mathbf{b}} = \nabla\times(\mathbf{v}\times\mathbf{b}) + \nabla\times(\eta\mathbf{j}) \tag{2}$$

$$\dot{p} = -(\mathbf{v}\cdot\nabla)\,p - \Gamma p(\nabla\cdot\mathbf{v}) + H \tag{3}$$

$$\dot{\rho} = -\nabla(\rho\mathbf{v}), \tag{4}$$

where v is the velocity, b the magnetic field, j the current density, η the resistivity, ν the viscosity, ρ the mass density, and p the pressure. H stands for a heat diffusion and an external heating term and is not further considered in this paper as it is not relevant for the numerical method.

The numerical scheme we will present is the same for cylindrical and toroidal geometry; but as in Section III we shall give only results for cylindrical tests we shall only provide explicit notations for this geometry. If toroidal geometry is considered, it will be specified explicitly.

In cylindrical tokamak simulations, we normalize the small radius to 1, the length of the device is $2\pi R_0$, the toroidal magnetic field at the center is $B_z(0) = R_0$, and the initial density is assumed to be a constant, $\rho = 1$; then the normalized Alfven time is $\tau_a = 1$. An equilibrium is defined by a pressure profile $p(r)$ and a safety factor profile $q(r)$, with $q(r) = rB_z/R_0 B$; q is of the order of unity and p generally of the order R_0^{-2}. The ideal MHD spectrum, obtained by solving the linearized equations around a static equilibrium, is divided into three distinct parts: the fast magnetoacoustic modes which form a discrete spectrum from $\omega \sim R_0$ to $\omega \sim R_0/\Delta r$, Δr being the small length scale considered; the shear Alfven waves form the second physically relevant part. They extend roughly from

$$\omega_a^2 = (m/q(r_\omega) - n)^2, \tag{5}$$

where m and n are the poloidal and toroidal mode numbers and form a continuous spectrum. The modes are peaked at r_ω, and the "resonant surfaces" of the configuration locate at $q(r) = m/n$. The third part is the slow sonic waves, whose velocities are along the field lines and $\omega^2 \sim \Gamma p$ (Γ being the ratio of the specific heats and p the pressure).

The physical resonances are defined by $q(r_s) = m/n$ and dominate the evolution in the sense that linear and nonlinear perturbations are mainly built up by shear Alfven modes near these surfaces, with small ω_a^2. The time scale of the nonlinear evolution remains of the order $1/\omega_a$. The amplitude of the nonlinear modes remains small, 10^{-2} is a typical value and 10^{-1} can be taken as an upper bound for a nonlinear kink or saturated tearing mode. As the dynamics is governed by resonances, these small perturbations have a tremendous influence on the magnetic configuration. Near the resonances, current sheets can appear, with typical width 10^{-2} and a maximum value of eight, up to ten times the equilibrium current.

We define S as $1/\eta(0)$, $\eta(0)$ being the resistivity at the center. Physical values of S can be as high as 10^9 (for some devices even higher), but 3D simulations with $S \sim 10^7$ are still quite difficult. In this case, a diffusive phase with very small magnetic perturbations requires about $10^5 \tau_a$; this indicates clearly that a linear unconditional stable scheme is required. On the other hand, the scheme has to permit a great spatial accuracy in the nonlinear phases (whose time scale is about $10^3 \tau_a$), conjugated with a time step not less than a fraction of τ_a, since the CPU time per time step is of the order of one second. We have tried to reconcile all these requirements in the semi-implicit method we shall now detail.

II.B. *The Semi-Implicit Method*

Following Ref. [8], we define a semi-implicit method by replacing the equation of motion for the velocity field $v = F$ by

$$(1 - \mathbf{L})v = F, \tag{6}$$

where $\mathbf{L}$ is a numerically stabilizing operator. In Refs. [9, 10] successive improvements of $\mathbf{L}$ have been presented, the best choice being an anisotropic

elliptic operator which dominates the explicit part (see Ref. [10], where the operator $\mathbf{L}$ is given explicitly in the Appendix).

We propose to use $\mathbf{L} = \Delta t^2 \mathbf{L}_0 + c\Delta$, where $\mathbf{L}_0$ is the full linearized MHD force operator around the equilibrium, Δ the Laplacian operator, and c is chosen such as to dominate only the nonlinear magnetic perturbations.

The exact definition of $\mathbf{L}_0$ is the following: using the MHD equation and linearizing them around an equilibrium, we obtain, by eliminating the B field and the pressure, a second-order equation for the velocity:

$$d^2v/dt^2 = \mathbf{L}_0 v.$$

$\mathbf{L}_0$ contains all the equilibrium quantities, toroidal and poloidal B fields, and pressure. It results, in the cylindrical case, in 1D matrices (diagonal in m and n) and, in the toroidal case, in 2D matrices (diagonal in n only).

This semi-implicit operator together with a second-order predictor corrector time-stepping to be discussed further in Section III.C ensures, in the linear phase, unconditional stability and, with finite but small c, good nonlinear stability properties together with a high spatial accuracy. Apart from the exact numerical scheme this provides in fact a linearly fully implicit scheme. The magnitude of c is small (typically 10^{-4}) and thus $c\Delta$ does not lower accuracy on linear modes, as c is independent on the time step, which can be very high in linear phases. We refer to III.C for a discussion of linear numerical stability and we will now discuss nonlinear stability (the time step is, in any case, limited by an CFL constraint on convection).

We will base our discussion of the nonlinear stability of the method on Ref. [9], where calculations are done for a uniform magnetic equilibrium field. Harned and Schnack showed first that for a constant magnetic field B_0 a semi-implicit operator

$$\mathbf{K}_0 = \Delta t^2 [\nabla \times \nabla \times (v \times \mathbf{C}_0)] \times \mathbf{C}_0 \tag{7}$$

with $\mathbf{C}_0$ colinear to B_0 and $|\mathbf{C}_0| \geqslant B_0$ would suffice to ensure numerical stability. $\mathbf{K}_0$ is just the linearized MHD force operator in the case of a constant magnetic field if $\mathbf{C}_0 = B_0$. Then they added a magnetic field B_1 perpendicular to B_0 and showed that stability is now ensured with $\mathbf{L} = \mathbf{K}_0 + \mathbf{K}_1$,

$$\mathbf{K}_1 = \Delta t^2 [\nabla \times \nabla \times (v \times \mathbf{C}_1)] \times \mathbf{C}_1, \tag{8}$$

provided that $\mathbf{C}_1$ is colinear to $\mathbf{B}_1$ and $|\mathbf{C}_1| \geqslant B_1$.

In our case, the equilibrium field plays the role of B_0 and $\mathbf{L}_0$; the full linearized MHD operator around the equilibrium plays the role of $\mathbf{K}_0$. This corresponds to the case where $\mathbf{C}_0 = B_0$, resulting in unconditional linear stability. The helical perturbation plays the role of B_1 and $\mathbf{L}_1 (c\Delta)$ plays the role of $\mathbf{K}_1$. For this situation we find, from Eq. (8) with $|\mathbf{C}_1| \geqslant B_1$, that nonlinear stability is ensured roughly if

$$c \geqslant (\Delta t\, \delta B)^2, \tag{9}$$

where δB is the size of the helical perturbation around the equilibrium. $\sqrt{c}$ can be interpreted as a smoothing length. Therefore we proceed as follows:

— we choose the smoothing length (say, $\sqrt{c} \sim 10^{-2}$)

— we adjust the time step such that (9) is fulfilled.

The tokamak configuration imposes a strong ordering of the components of the magnetic field such that $\delta B \ll B_0$; for example, during a sawtooth $\delta B \sim 10^{-2}$ gives a good order of magnitude. That is the reason why we are able to perform computations with a time step of the order τ_a, without losing spatial precision, as is demonstrated in Section III: c is about 10^{-4}, and this value cannot affect the spatial precision of the computation. In general, for about 100 grid points the mesh size is of the order of 10^{-2} so that nonlinear stability could be expected superficially without the semi-implicit term $c\Delta$. However, one has to bear in mind that:

— in the reconnection layer, a mesh size of $\Delta r \sim 10^{-3}$ is necessary to resolve a layer width of 10^{-2}; consequently grid accumulation has to be done. A factor of 10 for the time step is gained by use of the semi-implicit term to ensure nonlinear stability.

— near the center a very strong nonlinear instability takes place. We refer to III.A for a more thorough discussion. Once again the semi-implicit Laplacian operator provides more than a factor of 10 for the size of the time step in internal kink simulations.

In practice, we impose condition (9) only on the radial component δB_r. The reason is that the magnitude of the magnetic field is less important than its direction, and the departure of the latter from equilibrium comes from this component, δB_r. In all the runs we have made until now, we have never seen any non-linear numerical instability when (9), together with CFL velocity criterion, are fulfilled, even near large current sheets such as those shown in Section III. The reason is probably that these current sheets do not much change the nonresonant shear waves that are implicitly strongly stabilized. The resonant shear waves are obviously changed, but they evolve on a slow time scale and cannot lead to numerical instabilities. Neverthless, we have no precise criterion about that and keep in mind this potential trouble.

In cylindrical geometry, this method is not more expensive in computing time than the original semi-implicit one, as the semi-implicit operator has the same diagonal structure for the m, n Fourier modes. In toroidal geometry this is no longer true: for a given n all the m are coupled and the implementation is therefore much harder. But, nevertheless the matrices remain 2D, bloc tridiagonal, and in contrast to a purely implicit method, they need to be computed and decomposed only every N time steps (N being of the order of 100). Therefore the extra costs are not very high, typically 50% for 10 poloidal and 10 toroidal modes.

II.C. *Numerical Scheme*

We have developed a second-order predictor corrector scheme, where in contrast to the semi-implicit schemes presented in Ref. [8–10], we apply the stabilizing implicit operator **L** both at the predictor and corrector levels. This greatly improves the nonlinear stability of the code. Thus, the scheme reads (omitting the temperature diffusion and heating terms):

Predictor.

$$\begin{aligned}(1-\mathbf{L})(v^*-v_n)&=\frac{\Delta t}{2}F_v(v_n, b_n, p_n)\\ b^*-b_n&=\frac{\Delta t}{2}F_b(v^*, b_n, p_n)\\ p^*-p_n&=\frac{\Delta t}{2}F_p(v^*, b^*, p_n);\end{aligned}\tag{10}$$

Corrector.

$$\begin{aligned}(1-\mathbf{L})(v_{n+1}-v_n)&=\Delta t\, F_v(v^*, b^*, p^*)\\ b_{n+1}-b_n&=\Delta t\, F_b\left(\frac{v_{n+1}+v_n}{2}, b^*, p^*\right)\\ p_{n+1}-p_n&=\Delta t\, F_p\left(\frac{v_{n+1}+v_n}{2}, \frac{b_{n+1}+b_n}{2}, p^*\right).\end{aligned}\tag{11}$$

Here, F_v, F_b, F_p denote the right-hand side of the MHD equations (1)–(4) on v, b, p, respectively. We omit ρ for simplicity, and the magnetic diffusion do not enter in F_b: an implicit resistive advance of B is performed after the corrector.

The linear stability of this scheme can readily be studied for a reduced model system, consisting of a two-dimensional eigenvector (v, b) of $\mathbf{L}_v$, as $\mathbf{L}=\Delta t^2\mathbf{L}_0$ in the linear phase, where c can be set to 0 for vanishing viscosity, $\nu=0$. Denoting $\mathbf{i}\omega$ the (complex) eigenvalue of this eigenvector (v, b) and $\alpha=\omega\,\Delta t$, we obtain a linear transfer matrix **T**,

$$\begin{pmatrix} 1-\dfrac{\alpha^2}{2(1+\alpha^2)} & \mathbf{i}\dfrac{\alpha}{1+\alpha^2}\left(1-\dfrac{\alpha^2}{4(1+\alpha^2)}\right)\\ \mathbf{i}\alpha\left(1-\dfrac{\alpha^2}{4(1+\alpha^2)}\right) & 1-\dfrac{\alpha^2}{2(1+\alpha^2)}\left(1-\dfrac{\alpha^2}{4(1+\alpha^2)}\right)\end{pmatrix}.\tag{12}$$

The determinant $\det(\mathbf{T})$ is $1-\alpha^4/8(1+\alpha^2)^2$; the discriminant $\Delta(\mathbf{T})$ remains positive. We find that the scheme is linearly unconditionally stable, second order in time and

with a fourth-order damping. However, this damping is a very selective one: fast modes, which correspond roughly to $\alpha \geqslant 10$, with a time step of order τ_a are damped, but shear Alfven waves, and particularly those relevant for the evolution (say $\alpha \leqslant 10^{-1}$) have negligible damping. In the nonlinear phase this scheme seems to be better than a standard implicit scheme (without a predictor), where v and B are inverted simultaneously. Moreover, the fact that the convection of the magnetic field is treated explicitly allows an easy improvement of the convectors if required (see III.D for an exemple).

Note that the coefficient in $\Delta t^2 \mathbf{L}_0$ is somewhat arbitrary. From det(**T**) it can be seen that a coefficient reduced up to $1/2\sqrt{2}$ (this leads to $1+\alpha^2$ being replaced by $1+\alpha^2/2\sqrt{2}$ in (12)) ensures the stability. However, increasing this coefficient certainly improves the nonlinear stability.

II.D. *Numerical Mesh and Boundary Conditions*

The variables are expanded in a Fourier series in the periodic coordinates θ and $\phi = z/R_0$, corresponding to poloidal and toroidal directions. Derivatives are calculated by using fast Fourier transforms with dealiasing options. In the radial direction we use two staggered meshes [5]; this is necessary for obtaining a correct linear MHD spectrum. Quantities v_r, b_r, J_θ, and J_z are defined on the integer mesh $r = (0, dr, ..., 1-dr, 1)$, where dr is the equidistant mesh size (in actual calculations an nonuniform grid is used); quantities v_θ, v_z, b_θ, b_z, J_r, ρ, and p are defined on the half-integer mesh $r = (-dr/2, dr/2, ..., 1+dr/2)$. Quantities on the half-integer mesh at $r = -dr/2$ are defined by parity considerations [5], together with (v_r, b_r) at $r = 0$, defined from (v_θ, b_θ) at $r = dr/2$ [9]. We use as boundary conditions at the wall $v_r(r=1) = 0$ and $b_r(r=1) = 0$. For nondissipative MHD no further conditions at the wall are required. With finite values for resistivity and viscosity, we impose $(\nabla \times v)_\theta = (\nabla \times v)_\phi = 0$ and $J_\theta = J_z = 0$ at $r = 1$, except for the $m = 0$, $n = 0$ components in cylindrical and the $n = 0$ components in toroidal geometry, where the total current is imposed.

II.E. *Comparison with Previous Schemes*

As for the FAR code [6], our scheme is linearly fully implicit. But there are two major differences between the scheme proposed here and that used in FAR code. First, we do not use explicit diffusive terms to stabilize the system nonlinearly, but a small implicit term. Second, we work in direct (v, b) quantities, while FAR works in potential representation. As stated in Ref. [6], this leads to difficulties in boundary conditions and in the inversion of implicit systems. As a result, Ref. [6] indicates a few tens of minutes (on a CRAY II) for a linear result, while we need a few minutes only in the same conditions, in the fully toroidal case (not presented here). Furthermore, we do not know if the fully algorithm used in FAR could be transposable in (v, b) quantities, free of the above time consuming difficulties.

The difference between our scheme and previous semi-implicit schemes is clear: for a given time step, we need a semi-implicit elliptic $c\Delta$ operator much smaller ($c = 10^{-3}$–10^{-4}) in size than that used in Refs. [8–10], as it stabilizes only the

departure of B from equilibrium (in linear cases, we need no semi-implicit elliptic operator at all). As a result, it seems unnecessary to optimize the form of this operator, using anisotropic elliptic operators as in Ref. [10] which would correspond otherwise to the case $c = 1$ for sime step of order τ_a. Note that even with this optimization, the velocity in boundary layers is very smoothed. On the contrary, the fully linearized MHD operator $\mathbf{L}_0$ does not unacceptably smooth the boundary layers, as its nearly vanishes on the resonant shear Alfven waves.

III. Numerical Test

III.A. *The nonlinear numerical instability of the center*

First we want to discuss a nonlinear numerical instability associated with any kinked situation and which is potentially relevant in the numerical tests presented in III.C and III.D. A shift of the center of the magnetic configuration is caused by a $m = 1$, $n = 1$ magnetic perturbation as all other, higher harmonics vanish at the center.

In the notation of II.A, and for a $m = 1, n = 1$ kink, the magnitude for the mode is

$$B_r = (1 - q(0))\xi, \tag{13}$$

where ξ is the shift of the magnetic axis. Around the center, the situation is then quite close to that discussed in II.B; an "equilibrium" field B_0 is perturbed by a nearly constant field. Consequently, without the semi-implicit $c\Delta$ term, a numerical instability is observed when

$$B_r \, \Delta t \approx \varepsilon.$$

But ε is in this case the gridding near the center. More precisely, it can be easily seen that the relevant value of ε near the center is dr/M, instead of simply the radial mesh size dr, as terms $(m/dr)^2$ enters in linear operators such as those defined by (7). For calculations with about $M = 10$ poloidal harmonics involved, one would get a drastic reduction of the time step: for $\xi = 0.5$ (i.e., in the middle of a resistive reconnection of the internal kink) and $1 - q(0) = 0.1$, the time step would be $0.02\,\tau_a$ for $M = 20$ and $dr = 10^{-2}$.

With the inclusion of the $c\Delta$ term, the analysis of II.B is quite precise for this simple effective geometry near the center and the condition

$$B_r \, \Delta t < \sqrt{c} \tag{20}$$

is sufficient to ensure numerical stability in any case. For example, the internal kink simulation presented below is run with time steps typically $0.3 - 1\tau_a$ (generally limited by a CFL criterion on convection) with a value of $c \approx 3 * 10^{-4}$. This value

cannot change the computation, as the smoothing is done over one grid cell dr, but a factor of M ($=10$) is gained for the time step.

In general, the criterion (20) is imposed over the whole domain, but an inhomogenous $c(r)$ is then used; c will typically be 10^{-4} in the resonant layers. Note that such an inhomogenous semi-implicit term has to be defined in a self-adjoint way, as has been pointed out by Mikic in Ref. [11].

III.B. *Nonlinear Tearing Mode Saturation*

As a first example of a practical application we consider an $m=2$, $n=1$ tearing mode. The tearing mode unstable equilibrium [12] is given by the profile of the safety factor $q(r)=1.4(1+(2r)^4)^{1/2}$ and an S value of 10^5, the viscosity is set to zero and 16 poloidal and 8 toroidal harmonics are used. Figure 1 shows the time evolution of the component B_r of the magnetic field of the $m=2$, $n=1$ mode. A time step of $\Delta t=10\tau_a$ was used in the linear phase and of $\Delta t=2\tau_a$ in the nonlinear, saturation phase, after time $t=800\tau_a$. As expected, even with this large time step the linear growth rate is quite precise: we find $\gamma=8.1\times10^{-3}\tau_a^{-1}$, the result from a linear finite element spectral code is $\gamma=7.95\times10^{-3}\tau_a^{-1}$. This has to be compared with Ref. [9], where it is stated that for such a large time step $\Delta t=10\tau_a$ the accuracy is poor. On Fig. 2 the velocity pattern is drawn: one can see that the saturated island is quite large and that, as expected, the velocity is extremal on the separatrix. This computation was made with absolutely no viscosity which explains the secondary vortices seen in the figure.

III.C. *Saturation of the Ideal Kink Mode*

The saturation of the ideal kink mode was predicted analytically by Rosenbluth *et al.* [13] and later confirmed numerically by Park *et al.* [14], using reduced MHD equations. The saturation of this ideal mode is accompanied by the forma-

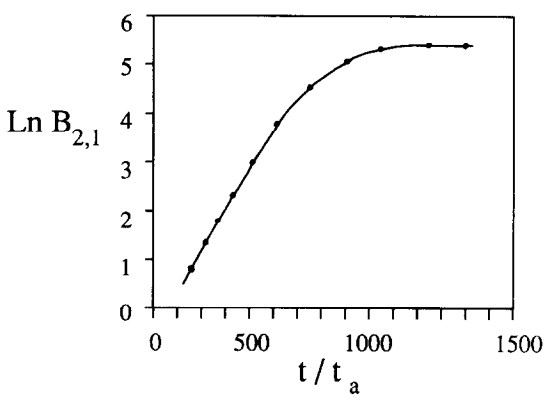

FIG. 1. The amplitude of the ($m=2$, $n=1$) magnetic component B_r (on a logarithmic scale) is plotted versus time.

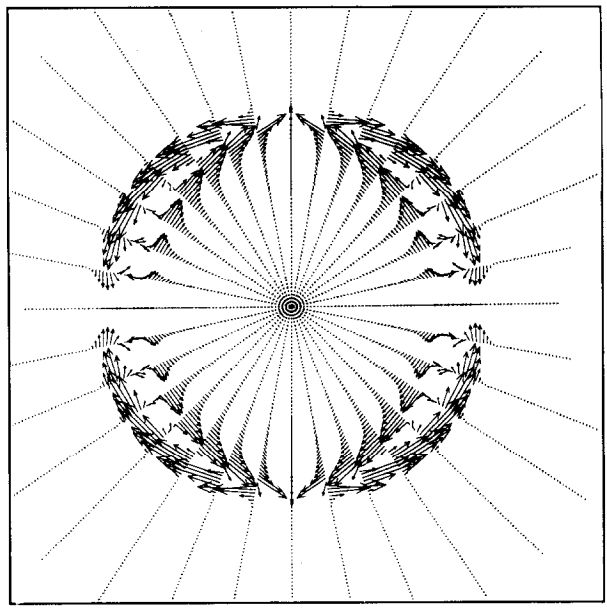

FIG. 2. Velocity pattern at time $t = 800\tau_a$.

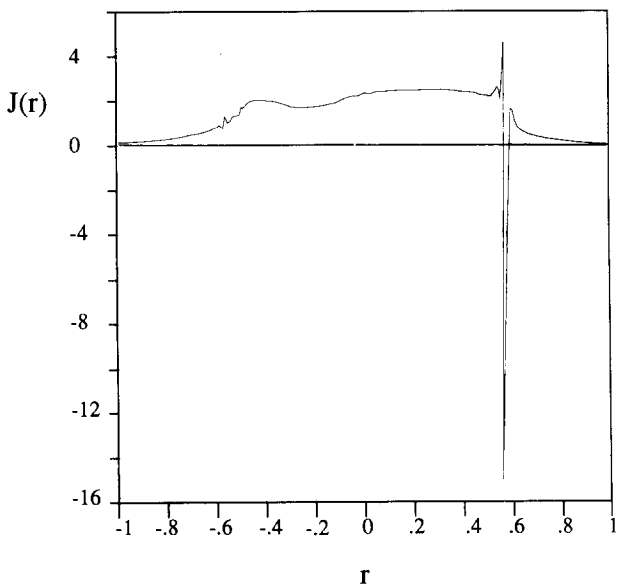

FIG. 3. Current profile of the saturated kink.

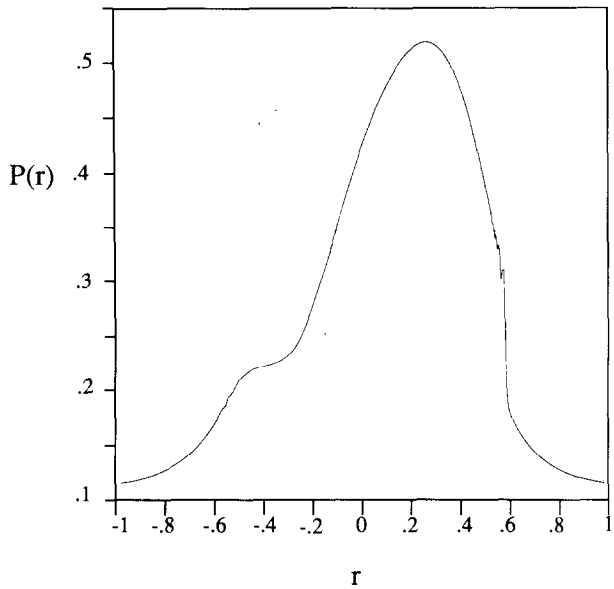

FIG. 4. Pressure profile corresponding to Fig. 3.

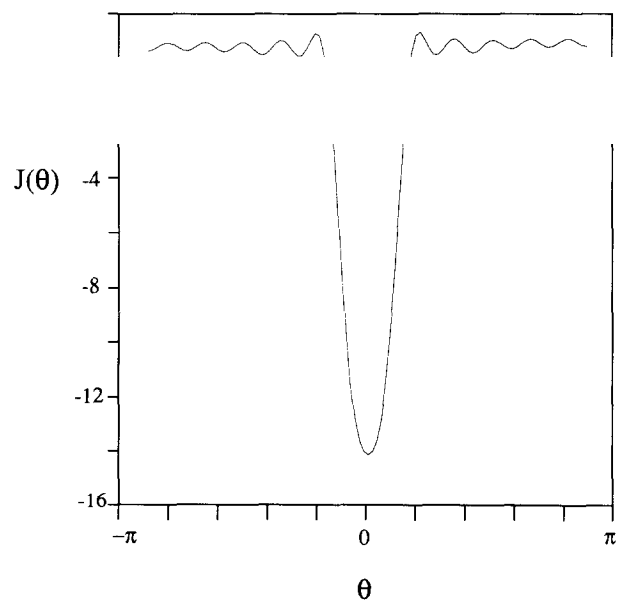

FIG. 5. Poloidal dependance $J(\theta)$ of the current spike shown in Fig. 3, from $\theta = -\pi$ to $\theta = \pi$.

tion of a singular current sheet on the surface defined by $q(r_s) = 1$; this raises serious difficulties for numerical calculations and constitutes an interesting, challenging test for a nonlinear code.

We studied the saturation of the internal kink for an equilibrium given by the q profile $q(r) = 0.9(1 + (r/r_0)^4)^{1/2}$, with $q(0.5) = 1$, and a high pressure ($\beta_p \sim 1$); at the end of the linear phase, quite a high viscosity ($v = 10^{-4}$) is added in order to dissipate the MHD energy which is transformed in kinetic Alfven waves energy near the resonant surface. The current and the pressure profile of the quasi-stationary state which then appears are represented in Fig. 3 and Fig. 4. One notes a deep, extremely thin current peak, eight times the main current (we use here a variable grid, $\Delta r \approx 10^{-3}$ in the resonant layer). In Fig. 5 we have plotted the poloidal dependence $J(\theta)$ in the current sheet. The simulation was run with only 12 harmonics, which explains the residual oscillations; nevertheless, the radial as well as the poloidal structure of the current sheet are satisfactory.

Numerically, we use for c a value of 10^{-4} and we note that this value does not change the thinness of the peak at all; in this ideal case, the velocity is rather large, and time step is limited by the convective CFL criterion.

III.D. *Resistive Reconnection*

As a last physically relevant test case we shall present a resistive reconnection for the same q profile as in Section III.C, but this time with zero pressure. We show in Figs. 6a,d the current profile and in Figs. 7a,d the isocontours of the helical flux,

$$\psi(r, \theta) = \int_0^r dr' \left(b_\theta - \frac{r'}{R_0} b_z \right)$$

at four different times in order to visualize the magnetic island during reconnection. We used here for S a value of 10^5 and viscosity was set at $v = 5 \times 10^{-5}$. Furthermore, we used a variable grid ($\Delta r = 2 \times 10^{-3}$ around the resonant surface) and 12×12 real modes were retained in the calculation; this corresponds to the "operational conditions" of the code. Initially, the time step here is $3\tau_a$ during the linear phase; then during the whole reconnection it is limited by the CFL constraint on convection: in this case, no limitation arises from the magnetic field (again we used $c = 10^{-4}$ in the current sheet and $c = 3 \times 10^{-4}$ at the center, which does not disturb the physical process). In this case, the scheme presented in II.C has been slightly modified: concerning the convection of the magnetic field, the predictor is decentered in order to assure the stability of the convection scheme under the CFL criteria (however, the predictor remains centered for the MHD part, where two values of B^* are calculated, one centered, the other one decentered).

The whole reconnection process takes about 1000 time steps, corresponding to about 40 min of CPU time on a CRAY 2 computer. In cylindrical geometry the reconnection is limited to single helicity and the utilization of the FFT is not

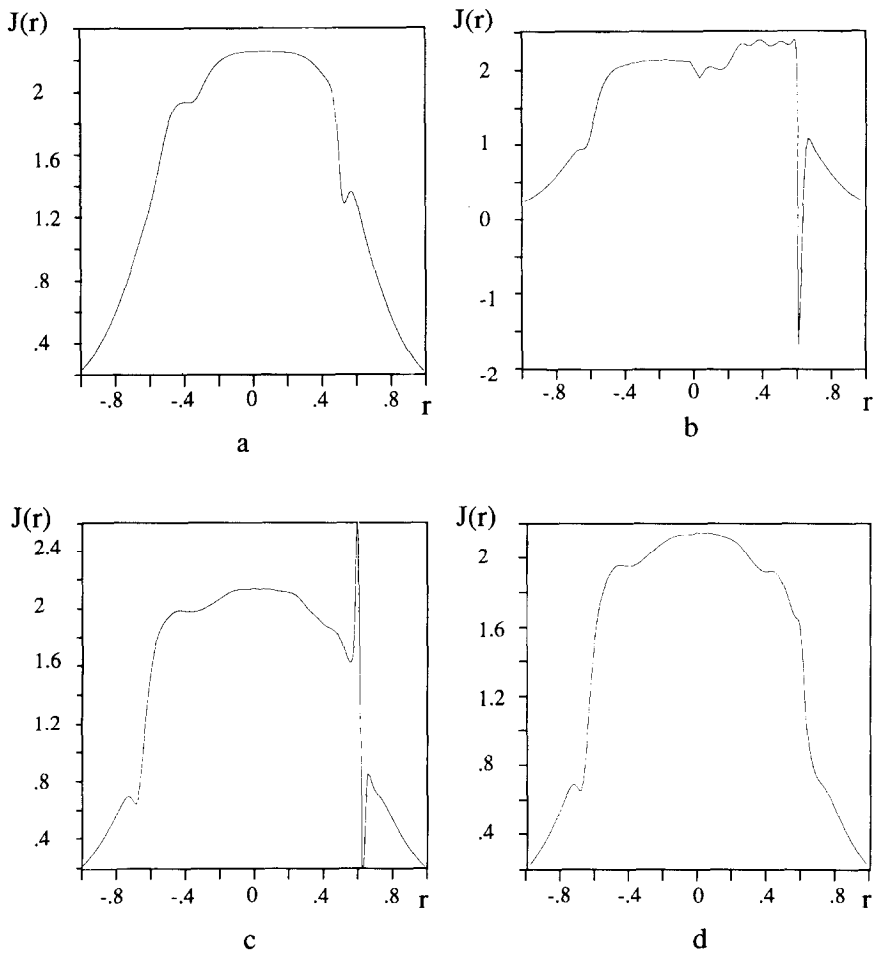

FIG. 6. Current profile during the resistive reconnection, at four different times: (a) $t = 228\tau_a$ during the linear growth phase; (b) $t = 409\tau_a$, in the middle of the reconnection; (c) $t = 507\tau_a$, where the current sheet disappears; (d) $t = 519\tau_a$, final state: a kink in the opposite direction takes place, as the reconnection was not complete.

appropriate. However, we want to stress the fact that we are ultimately interested in studying these effects in toroidal geometry where different helicities are coupled.

We do not present here the results for higher S values. Let us simply point out that the number of time steps necessary for a reconnection does not increase as long as the time step is limited by convection—this seems to be the case for S values between 10^6 to 10^7. Regarding our preliminary results, we hope to be able to work with an S value higher than 10^7 and with current sheets comparable to the ones found in Section III.C. Such a run would take about 2 h of CPU time for the study of very nonlinear behaviour.

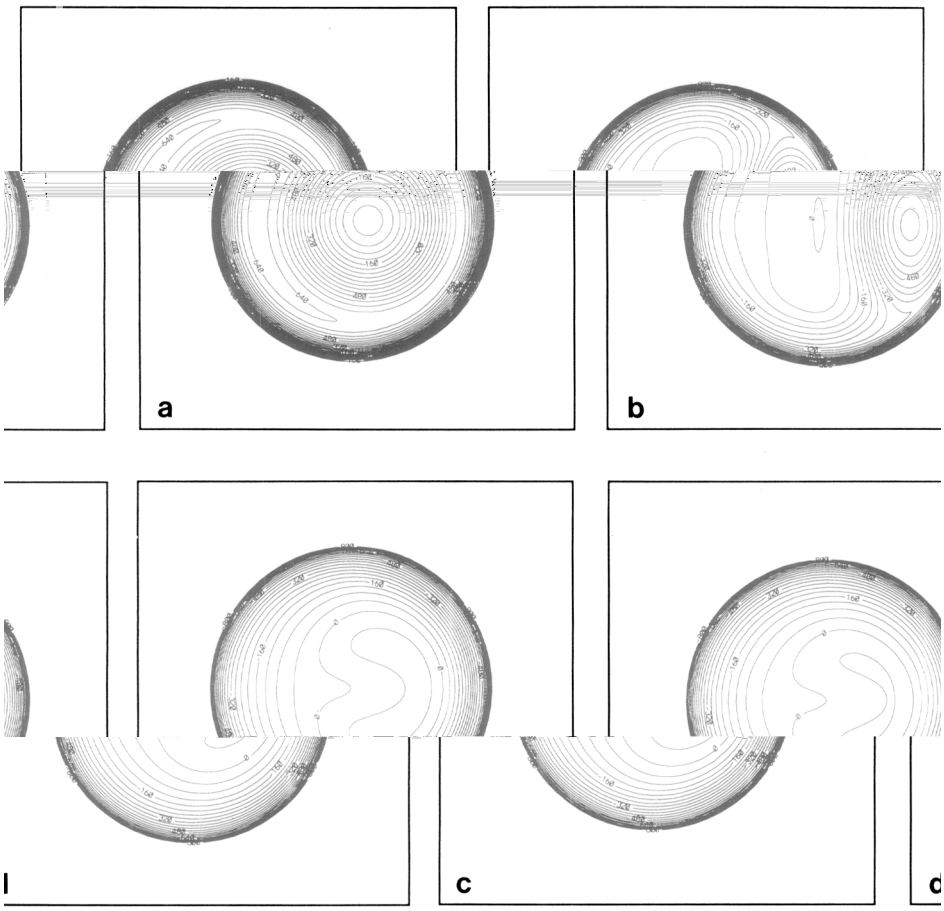

FIG. 7. The helical flux at the same times as in Fig. 6.

IV. CONCLUSION

The test cases presented in Section III show that the proposed scheme does answer to the fixed objective, to allow simulation of the MHD phenomena with a reasonable CPU cost (about 1 h for quite a high number of modes, typically 12×12). More precisely, this scheme allows a high spatial resolution of radial boundary layers with a reasonable large time step: unlimited in the linear or diffusive phases, about 1 to $0.1\tau_a$ in very nonlinear phases, i.e., with important deformations of the magnetic configuration accompanied by current peaks. The main advantage of this method lies in the fact that the time step is adjusted to the physical time scale to be studied. For this reason, this method is quite useful for tokamak

configurations where the field is constrained and where the separation of time scales is large. The method, for example, would be less useful for the reversed-field pinch configuration, where the dynamics are rapid. It is, of course, more difficult to implement this scheme than the semi-implicit schemes proposed so far, especially in toroidal geometry. Furthermore, it is more expansive as far as CPU time is concerned, but we strongly believe that it is far less expensive for a given precision. In fact, the inversion of the 2D operator in toroidal geometry is not very time consuming: the operators are bloc tridiagonal, each bloc of size $7 \times M$, so that for $M \sim 10$ the vectorization becomes quite efficient. We hope to be able to present, in the near future, the corresponding test cases for toroidal geometry.

ACKNOWLEDGMENTS

The authors are grateful to J. C. Adam and A. Heron for many valuable discussions and they have greatly benefitted from an enjoyable collaboration with M. N. Bussac and R. Pellat. One of the authors (K. L.) was supported by a grant from EURATOM. Calculations were performed at the Centre de Calcul Vectoriel pour la Recherche.

REFERENCES

1. H. R. STRAUSS, *Phys. Fluids* **19**, 134 (1976).
2. B. V. WADDELL, M. N. ROSENBLUTH, D. A. MONTECELLO, AND R. B. WHITE, *Nucl. Fusion* **16**, 528 (1976).
3. H. R. HICKS, B. CARRERAS, J. A. HOLMES, D. K. LEE, AND B. V. WADDELL, *J. Comput. Phys.* **44**, 46 (1981).
4. R. IZZO, D. A. MONTICELLO, H. R. STRAUSS, W. PARK, J. MANICKAM, R. C. GRIMM, AND J. DELUCIA, *Phys. Fluids* **26**, 3066 (1983).
5. A. Y. AYDEMIR AND D. C. BARNES, *J. Comput. Phys.* **53**, 100 (1984).
6. L. A. CHARLTON, J. A. HOLMES, V. E. LYNCH, B. A. CARRERAS, AND T. C. HENDER, *J. Comput. Phys.* **86**, 270 (1990).
7. A. Y. AYDEMIR AND D. C. BARNES *J. Comput. Phys.* **59**, 108 (1985).
8. D. S. HARNED AND W. KERNER, *J. Comput. Phys.* **60**, 62 (1985).
9. D. S. HARNED AND D. D. SCHNACK, *J. Comput. Phys.* **65**, 57 (1986).
10. D. D. SCHNACK, D. C. BARNES, Z. MIKIC, D. C. HARNED, AND E. J. CARAMANA, *J. Comput. Phys.* **70**, 330 (1987).
11. Z. MIKIC, 13th conf. on the numerical simulation of plasma, Santa Fe, NM, 1989.
12. H. P. FURTH, P. H. RUTHERFORD, AND H. SELBERG, *Phys. Fluids* **16**, 1054 (1973).
13. M. N. ROSENBLUTH, R. Y. DAGAZIAN, AND P. H. RUTHERFORD, *Phys. Fluids* **16**, 1894 (1973).
14. W. PARK, D. A. MONTICELLO, R. B. WHITE, AND S. C. JARDIN, *Nucl. Fusion* **20**, 1181 (1980).